Astron. Astrophys. 325, 819–824 (1997)

ASTRONOMY
AND
ASTROPHYSICS

Speckle measurements of the centre-to-limb variation of the solar granulation

V. Wilken[1], **C.R. de Boer**[1,2], **C. Denker**[1], **and F. Kneer**[1]

[1] Universitäts-Sternwarte, Geismarlandstr. 11, D-37083 Göttingen, Germany
[2] Max-Planck-Institut für Aeronomie, Max-Planck-Straße 2, D-37189 Katlenburg-Lindau, Germany

Received 6 January 1997 / Accepted 1 April 1997

Abstract. The Vacuum Tower Telescope (VTT) at the Observatorio del Teide/Tenerife was used to perform speckle observations of photospheric granulation from disc centre to limb at $\lambda = 550 \pm 5$ nm. Images were reconstructed with the spectral ratio technique (von der Lühe 1984) and the speckle masking method (Weigelt 1977, Weigelt & Wirnitzer 1983, Lohmann et al. 1983).

The granular rms contrast relative to the local average intensity decreases monotonically from $13.5 \pm 1.0\%$ at disc centre to 8–9 % at $\cos\vartheta = 0.1$. The granular images as well as the power spectra of the intensity fluctuations show a fading of the coarse granular pattern towards the limb while smaller structures become more pronounced off the disc centre. We identify these as the bright worm-like structures appearing sometimes at the granular borders (de Boer et al. 1992). This finding supports the result from simulations of granular dynamics by Steffen et al. (1994). There the bright structures are locations of low pressure between the centres of granules and intergranular spaces with penetration of hot gas into the lower photosphere.

Key words: Sun: granulation, centre-to-limb variation – techniques: speckle interferometry

1. Introduction

Observations of the centre-to-limb variation (CLV) of solar phenomena enables us to study the height variation of the atmospheric structures and dynamics on the Sun. The present investigation deals with the CLV of the granular intensity contrast. This gives information on the process of convective overshoot into the lower solar atmosphere (we refer the reader to the monograph by Bray et al. 1984 and to the review by Spruit et al. 1990). Komm et al. (1990, 1991a, 1991b), Nesis et al. (1988), and Vollmöller et al. (1996), among many others, have used spectroscopic observations to study the height variation of granular dynamics including velocities. They found that the granular phenomenon reaches to heights of approximately 150 km (above $\tau_{5000} = 1$). Surprisingly, the smaller structures penetrate higher than large patterns. Secondary processes are excited above 150 km by the convection.

Sophisticated numerical simulations of the granular convection have been performed among others by Cattaneo et al. (1989), Malagoli et al. (1990), Nordlund & Stein (1989), and Steffen et al. (1994). On the one hand computed intensity and velocity patterns agree with measurements of the Sun, on the other hand some features still need clarification. For instance, the simulations show bright rims at some borders of granules (e.g. Malagoli et al. 1990, Steffen et al. 1994). Such brightenings have indeed been identified by de Boer et al. (1992) from speckle observations. Their origin is yet unclear. From simulations performed by Malagoli et al. (1990) they could arise from shocks due to fast horizontal motions of granular material into cool intergranular lanes. Nesis et al. (1992) searched for observable post-shock turbulence at the granulation - intergranulation interface. Unlike Malagoli et al. (1990) the calculation of Steffen et al. (1994) gives increased convective upflow at granular borders, i.e. increased intensity, due to low pressure there (cf. also Solanki et al. 1996). In the present paper we will show observations that support the latter alternative.

Measurements of the CLV of the granular intensity contrast have been presented by Wiesmeier & Durrant (1981). They used data obtained with the balloon-borne German Spektrostratoskop (Mehltretter et al. 1978) which had an aperture of $D = 30$ cm. Karpinsky (1990) presented excellent results from the Soviet Stratospheric Solar Observatory (also balloon-borne, $D = 50$ cm). More recently, Rodríguez Hidalgo et al. (1992) have analysed observations from the Swedish Solar Tower ($D = 50$ cm) on La Palma (numerous references on measurements of granular contrast are given in their work). Assuming that the granular pattern is flat, i.e. it has no height extension, and that radiative transfer effects do not play any role when observing at various heliocentric angles, Rodríguez Hidalgo et al. (1992) inferred the value of the Fried parameter r_0 which is a measure of the seeing quality.

Send offprint requests to: V. Wilken

Obviously, it is important to acquire the best available spatial resolution for studying the CLV of granular structures because the pattern is much foreshortened close to the limb. First investigations of the CLV using classical one-dimensional speckle interferometric techniques were performed by Harvey & Breckinridge (1973) and by Ricort & Aime (1979). Improved methods were applied by Druesne et al. (1989). Their approach does not compensate for seeing effects on the power spectra. Yet meanwhile, the speckle technique was established as a method which allows image reconstruction and which gives reliable results on solar fine structure (de Boer 1993, de Boer et al. 1992, de Boer & Kneer 1992, von der Lühe 1993, Denker et al. 1995, de Boer 1996) Therefore, it was natural to apply it to the CLV of granular structures. In the following sections we describe the speckle observations and their analysis and discuss the results for the granular CLV.

2. Speckle observations

The observations were obtained on September 1, 1993 with the Vacuum Tower Telescope (VTT, $D = 70$ cm) at the Observatorio del Teide/Tenerife. Four scans with six positions from disc centre to the north limb were taken starting at a heliocentric angle $\vartheta = 0^\circ$ and with steps of 18° in ϑ. Images close to the limb contain more than one position in $\cos\vartheta$. Active regions and plages were avoided. At each position a burst of 140 specklegrams was taken. The wavelength and bandwidth were $\lambda = 550$ nm and $\Delta\lambda = 10$ nm, respectively, and the exposure time for each frame was 4 ms. We used a slow-scan CCD system from LaVision with a 384×286 pixel chip TH7863FT from Thomson. The frame rate was 5 frames/s with a digitization depth of 12 bits. The image scale was $0\farcs08$/pixel, which is half of the diffraction limit $\alpha = \lambda/D = 0\farcs16$. In addition, dark frame bursts and flat field bursts, with the telescope out of focus, were taken for the data calibration. The corresponding field of view was approximately $31'' \times 28''$.

3. Speckle reconstruction of granulation images

Before employing the speckle methods (see e.g. de Boer et al. 1992, de Boer 1993), the frames were treated in the usual way: the dark signal was subtracted, the gain table was applied. Image motion was removed by cross-correlating the filtergrams to the one with the highest contrast. Then we divided the images into partially overlapping subfields with a size of 64×64 pixels. This area of $5\farcs12 \times 5\farcs12$ corresponds approximately to the size of the isoplanatic patch at the site. To determine the atmospheric point-spread function, we used the spectral ratio method of von der Lühe (1984) to derive the Fried parameter r_0. The latter turned out to be in the range of 10–14 cm for the present observations. Korff's (1973) model of the speckle transfer function (STF) and Fried's (1966) model of the average short-exposure modulation transfer function were applied to compare the observed spectral ratios $\varepsilon(\boldsymbol{q})$ with theoretical values where

$$\varepsilon(\boldsymbol{q}) = \frac{|\langle \mathrm{F}(\boldsymbol{q})\rangle|^2}{\langle|\mathrm{F}(\boldsymbol{q})|^2\rangle} = \frac{|\mathrm{F}_0(\boldsymbol{q})|^2}{|\mathrm{F}_0(\boldsymbol{q})|^2} \cdot \frac{|\langle \mathrm{S}(\boldsymbol{q})\rangle|^2}{\langle|\mathrm{S}(\boldsymbol{q})|^2\rangle} = \frac{|\langle \mathrm{S}(\boldsymbol{q})\rangle|^2}{\langle|\mathrm{S}(\boldsymbol{q})|^2\rangle} \quad . \quad (1)$$

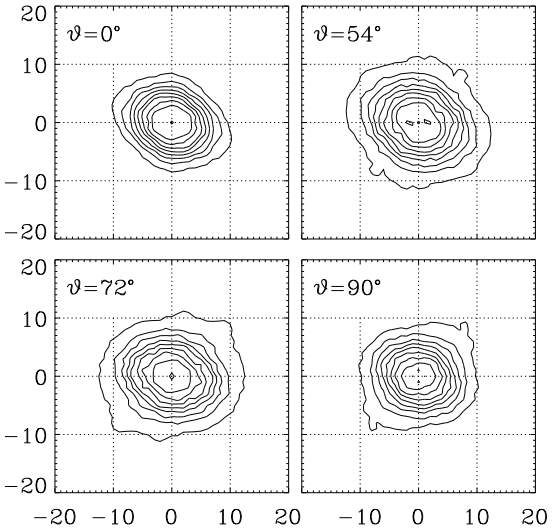

Fig. 1. Contour plots of the spectral ratios εobtained at various heliocentric angles.

Here, the brackets $\langle \quad \rangle$ denote ensemble averages. $\mathrm{F}(\boldsymbol{q})$ is the Fourier transform of an image at the two-dimensional wavenumber $\boldsymbol{q}$ and $\mathrm{F}_0(\boldsymbol{q})$ is the Fourier transform of the object's intensity distribution. $\mathrm{S}(\boldsymbol{q})$ is the instantaneous optical transfer function (OTF) of the object and $\langle|\mathrm{S}(\boldsymbol{q})|^2\rangle$ is the STF. A new filter (de Boer 1996) was used to suppress noise whose power spectrum was determined from the flat field bursts. Eq. (1) shows that $\varepsilon(\boldsymbol{q})$ depends only on the seeing, i.e. it contains no information on the object. To our knowledge, this was not yet confirmed by speckle reconstructions (of solar images).

In case that seeing effects, and instrumental aberrations, possess radial symmetry, i.e. are isotropic, Eq. (1) requires that $\varepsilon(\boldsymbol{q})$ be isotropic as well. This is approximately so in the example given in Fig. (1). It is of some concern that, in two out of the four centre-to-limb scans, $\varepsilon(\boldsymbol{q})$ exhibits increasing anisotropy towards the limb. For given constant ε the appertaining $\boldsymbol{q}$ describes an ellipse. The large axis of this ellipse is in the direction perpendicular to the limb. As a consequence, the Fried parameters r_0 calculated from the spectral ratios along the limb and perpendicular to it differ by 25–30% in the sense that seeing appears to be better perpendicular to the limb than parallel to it. For the moment, we don't know the cause of the ellipticity and why it changed from scan to scan. The problem surely asks for a clarification. Yet more data, taken under varying conditions, are needed for this porpose.

The amplitudes of the object's Fourier transform were corrected according to the classical method of Labeyrie (1970). The speckle masking technique (Weigelt 1977, Weigelt & Wirnitzer 1983, Lohmann et al. 1983, Pehlemann & von der Lühe 1989) was applied to the filtergrams to yield the phase of the object's Fourier transform. This highly redundant method allows the construction of a further noise filter, a reliability function determined from the scatter of the phases obtained at each point in the Fourier domain (de Boer 1996). After back-transformation

into object space, the restored sub-images of the observed object were reassembled.

Fig. 2 shows four examples of reconstructed granulation images at various heliocentric angles $\vartheta = 0°$, $\vartheta = 54°$, $\vartheta = 72°$, and at the limb. The smallest bright, dot-like structures in the intergranular space exhibit a halfwidth of $0\farcs2$. The substantial improvement of quality of the reconstructed images compared to the best single frames can be seen in de Boer & Kneer (1992).

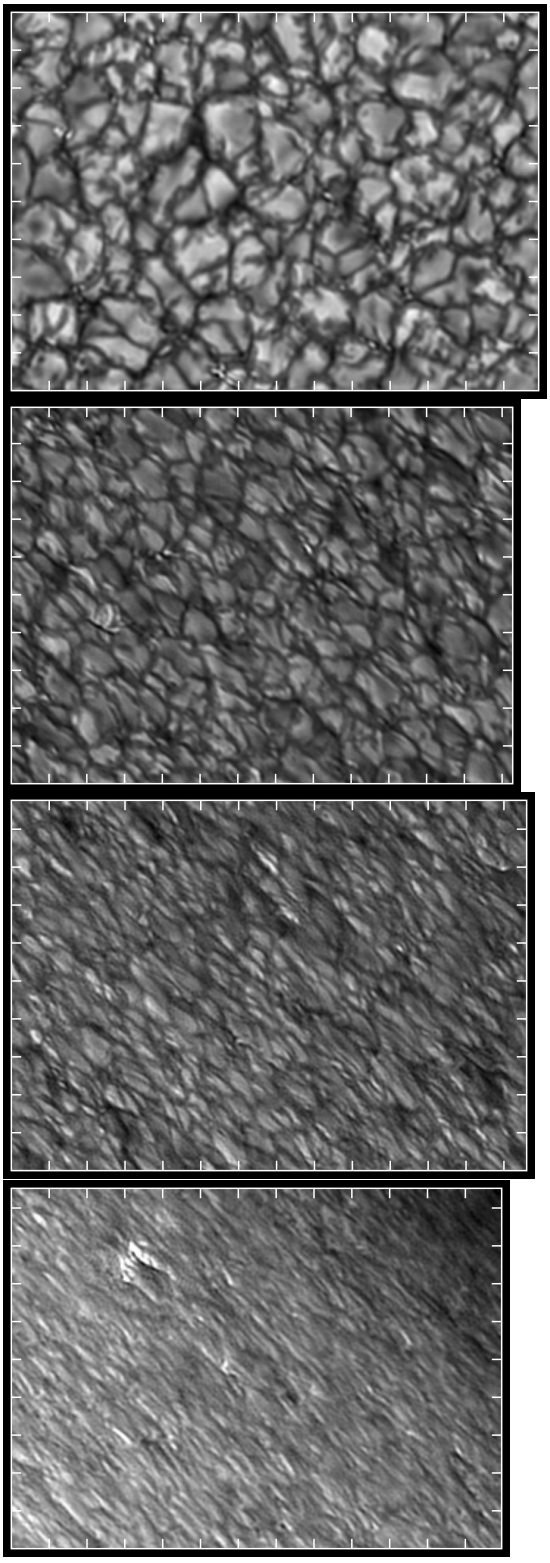

Fig. 2. Speckle reconstructions of the solar granulation (from top to bottom): at $\vartheta = 0°$, at $\vartheta = 54°$, at $\vartheta = 72°$, at the limb. The distance of the tick marks is equal to 2 ″.

4. Results and discussion

4.1. rms contrast

We compared the CLV of the relative average intensities $\overline{I}(\vartheta)/\overline{I}(\vartheta = 0)$ with the values at 550 nm from the Harvard Smithsonian Reference Atmosphere (HSRA, Gingerich et al. 1971). Only close to the limb ($\cos\vartheta \approx 0.1$), the intensities of the present data were higher by 10–12% than those from the HSRA. The same holds for the measurements of the CLV with careful corrections for false light and polynomial fits by Elste (1968), Neckel & Labs (1994), and Neckel (1996). The higher intensities close to the limb in our data are unlikely to be caused by changes of the sky transparency during the observation since this effect occurs in all centre-to-limb scans. Scattering of light in the Earth's atmosphere or at optical surfaces may also not be the reason for the higher intensities in our observations. Scattering tends to smooth the limb profile and this would lower the observed intensities close to the limb. We rather ascribe the discrepancy to the effect of not having observed in the true continuum but broadband. The interspersed spectral lines may effect a rise of the intensity near the limb relative to the disc centre intensity. At present, we have to accept the difference between our measured relative intensities and those from the specially designed and analysed measurements by e.g. Neckel & Labs (1994). Due to the uncertainty of the relative average intensity at the extreme limb, the intensity fluctuations given below will be uncertain by the same 10–12%.

Fig. 3 shows the CLV of the relative rms contrast $\Delta\mathrm{I}_{\mathrm{rms}}(\vartheta)/\overline{\mathrm{I}}(\vartheta)$. Lines connect the data points from different centre-to-limb scans to guide the eye. The results by Wiesmeier & Durrant (1981) are given for comparison. We obtain at the disc centre a rms fluctuation of 0.135 which is in good agreement with other measurements (cf. de Boer 1996). We note that at the disc centre the smallest structures contribute only little to the rms contrast. In our images the relative contrast decreases slowly towards the limb and reaches 0.08–0.09 for $\cos\vartheta = 0.07$. The Wiesmeier & Durrant (1981) data stay rather constant from the disc centre to $\cos\vartheta = 0.5$ and then decrease towards the limb. These results are of interest for comparison with contrasts obtained by numerical simulations of the granular dynamics. Furthermore we measured the rms contrast relative to the average intensity at the disc centre: $\Delta I_{\mathrm{rms}}(\vartheta)/\overline{I}(\vartheta = 0)$ decreases monotonically from 0.135 at disc centre to about 0.038 at $\cos\vartheta = 0.07$. We note that the rms contrast cannot be used in a straight forward sense to deduce a rms temperature fluctuation.

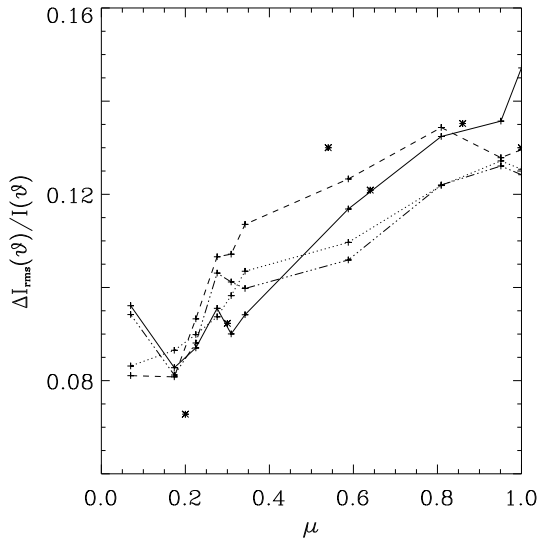

Fig. 3. Centre-to-limb variation of the relative rms contrast (with μ = cos ϑ). Lines connect the data points from different scans. The stars mark the results of Wiesmeier & Durrant (1981).

Kneer et al. (1980) have shown that an intensity increase due to an increase in temperature is partly 'eaten up' by an increased H^- opacity.

4.2. Power spectra

Let $I(x, y)$ be some two-dimensional intensity pattern in a sufficiently large area and $P(k_x, k_y)$ its power spectrum. We contract the area by a factor μ = cos ϑ along the y-axis such that we see the pattern under the angle of view ϑ. We suppose that the pattern is flat, i.e. has no dependence on the third co-ordinate z, and that the spatial resolution is sufficient so that the image is not degraded by the foreshortening. The pattern is then (see also Druesne et al. 1989)

$$I'(x, y) = I(x, y/\mu) \tag{2}$$

and its power spectrum is

$$P'(k_x, k_y) = \mu P(k_x, \mu k_y) \quad . \tag{3}$$

For $k_y = 0$, along k_x, the power spectrum is reduced by the factor μ:

$$P'(k_x, k_y = 0) = \mu P(k_x, k_y = 0) \quad . \tag{4}$$

Along k_y (for $k_x = 0$), it is also reduced by the factor μ but elongated by the factor μ:

$$P'(k_x = 0, k_y) = \mu P(k_x = 0, \mu k_y) \quad . \tag{5}$$

The integrated power remains conserved under foreshortening as it should. The granulation pattern is isotropic in quiet regions and so is the power spectrum of its intensity fluctuations. If only the angle of view influences the shape of the granular pattern the iso-power lines become elliptical due to foreshortening, with μ as the ratio of the axes in k_x and k_y. Here we use x and y as the orientation parallel and perpendicular to the limb. In reality, the images will be degraded due to a finite spatial resolution. We assume an isotropic modulation transfer function. We would then expect that the power along the short and the long axis of the ellipses coincide at the origin ($k_x = 0$, $k_y = 0$, cf. Eqs. 4, 5) and at large k_x and k_y due to limited spatial resolution.

Fig. 4 shows power spectra along the long (dash-dotted curves) and short (dashed curves) axis of the ellipses. The power spectrum from the disc centre is azimuthally averaged. The dotted curves at μ = 0.59, 0.34 and 0.17 are the expected spectra calculated from that at μ = 1.0 with foreshortening only (Eqs. 4 and 5). The vertical straight lines at k = 43.3 Mm^{-1} indicate a structural length of 0.″2 which is approximately the resolution limit of the images. The above expectations from foreshortening and degradation are partly reflected in the spectra: coincidence at small k and almost equal power values at large k; off the disc centre a larger power spectrum perpendicular to the limb than that parallel to the limb. Yet differences from the expectation are evident as well. Firstly, the total power decreases from the disc centre to the limb. This finding is identical to the result of the decreasing intensity fluctuation towards the limb (cf. Fig. 3). It is not much affected by limited spatial resolution since most power of the intensity fluctuation resides at small wavenumbers, i.e. large structures, even near the limb. Secondly, starting at μ = 0.59 and definitely closer to the limb, μ = 0.34 and μ = 0.17, the average slope of the power spectra parallel to the limb differs from that at μ = 1.0 (lower dotted curves). Small structures become more pronounced at the expense of large structures. This is different from the result obtained by Druesne et al. (1989). They find that the power spectra parallel to the limb fall off more rapidly near the limb than near disc centre. Close to the limb, the power spectra perpendicular to the limb (in Fig. 4) should be interpreted with caution because they suffer strongly from degradation at large k, even with a spatial resolution of 0.″2. For instance, at μ = 0.34, the structures of 1.″0 size are foreshortened to 0.″34 perpendicular to the limb.

In Fig. 5 we give the axis ratios of the iso-power ellipses at two different power levels, 2 10^{-6} and 1 10^{-7} (in arbitrary units). For the larger structural scales the ratio r follows closely the diagonal $r = \mu$ (= cos ϑ) down to $\mu \approx 0.3$. Closer to the limb we have $r > \mu$, possibly due to image degradation which affects essentially the power at high wavenumbers. For the smaller scales, those with less power, the degradation starts further away from the limb, at μ = 0.6–0.7. Image degradation is one explanation for the fact that r differs from μ close to the limb. Yet, in addition, radiative transfer effects and the details of the three-dimensional temperature and opacity structure may also become important for the intensity pattern when observing granular structures near the limb.

We return to the result of Fig. 4 that small structures become better visible near the limb in comparison to large structures. We interpret this as an effect of geometric height in the solar atmosphere. Using the Eddington-Barbier relation for the HSRA one sees radiation from atmospheric heights of 65 km and 105 km

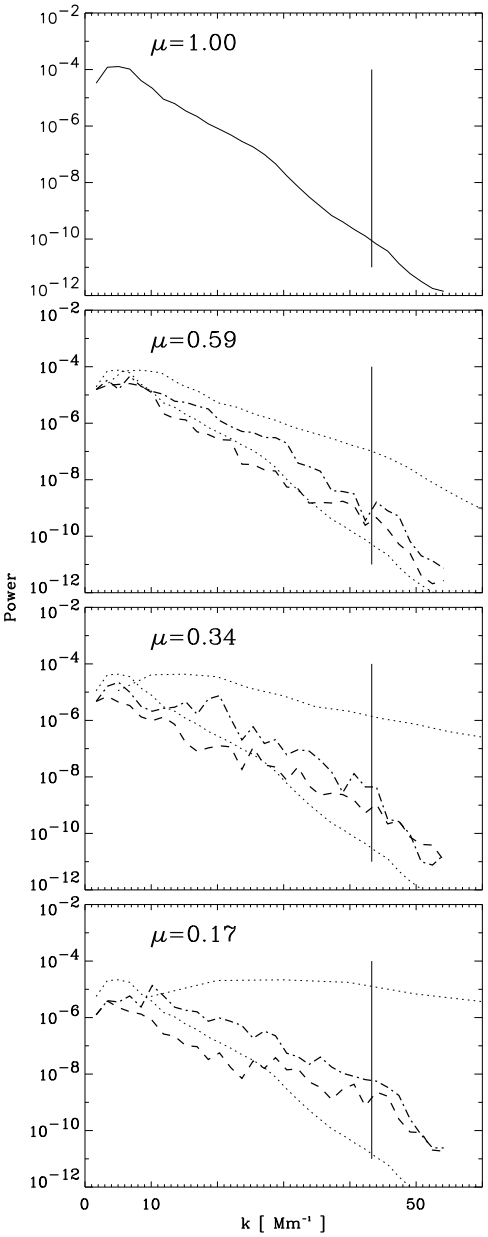

Fig. 4. Power spectra of the intensity fluctuations (in arbitrary units) at various heliocentric angles. Solid curve at μ = 1.0: azimuthally averaged power spectrum; dash-dotted and dashed: power spectra perpendicular and parallel to the limb, respectively; dotted: expected spectra calculated from that at μ = 1.0 with foreshortening only. The vertical straight lines at k = 43.3 Mm^{-1} indicate a structural length of 0.″2 which is approximately the resolution limit of the images.

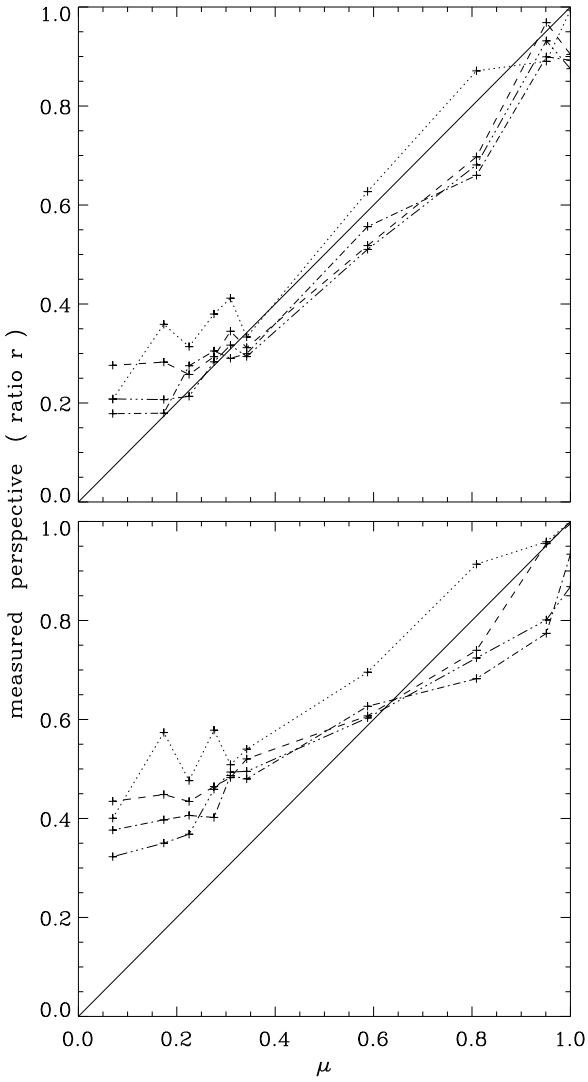

Fig. 5. Axis ratios of the iso-power ellipses at two different power levels, 2 10^{-6} (top) and 1 10^{-7} (bottom, in arbitrary units). Lines connect the data points from different scans.

for μ = 0.34 and μ = 0.17, respectively, compared to the height of 0 km for $\mu = \tau_{5000} = 1$. (At 550 nm the H^- bound-free absorption is larger by about 6% than at 500nm (Geltman 1962). This is of no relevance for the present coarse estimate of the height of formation.) Our finding thus agrees with that by Komm et al. (1990): Small granular structures penetrate into higher layers than the large granules, which is paradoxical. Here in the present study, we can identify the small structures off the disc centre. Inspection of the images in Fig. 2 for $\vartheta = 54°$ and for $\vartheta = 72°$ and comparing with the disc centre image we see that the coarse granular, 'convection-cell' pattern gradually fades away towards the limb while the short, 'worm-like' bright borders (de Boer et al. 1992) become the dominant features. Thus, although reproduced with the identical scale, the image from $\vartheta = 72°$ in Fig. 2 exhibits smaller structures than the disc centre image.

This is of relevance for the dynamics of granular convection. Our speckle observations support strongly the explanation of the bright granular rims by the simulations of Steffen et al. (1994). In this picture, the low pressure at positions between granular upflow and intergranular downflow allows, from time to time, enhanced transport of hot material into higher layers.

5. Conclusion

With speckle imaging providing a spatial resolution of approximately 0.″2 we could determine the CLV of the granular contrast at a wavelength λ = 550 nm. The relative rms-contrast decreases monotonically towards the limb – a fact which was known before. We believe that the accuracy achieved here is better than was feasible before. The values obtained should serve for comparison with predictions of the radiation calculated from granulation models.

A second important result concerns the CLV of the power spectra of the granular pattern in connection with the appearance of high-resolution images. Off the disc centre, the short bright granular rims (de Boer et al. 1992) become more pronounced than the coarse granular structure itselve. Our finding supports the picture by Steffen et al. (1994) that the bright borders stem from enhanced upflow of hot gas with penetration into photosheric layers well above τ = 1. Observations with high spatial resolution have again proven useful to scrutinize small-scale dynamical processes on the Sun.

Acknowledgements. Financial support by the Deutsche Forschungsgemeinschaft through grants Kn 152/12-1/2 and Kn 152/14-1 is gratefully acknowledged. The Vacuum Tower Telescope is operated by the Kiepenheuer-Institut für Sonnenphysik, Freiburg, at the Spanish Observatorio del Teide of the Instituto de Astrofísica de Canarias.

References

Bray R.J., Loughhead R.E., Durrant C.J., 1984, The Solar Granulation, 2nd edition, Cambridge University Press
Cattaneo F., Hurlburt N.E., Toomre J., 1989, Two- and Three-Dimensional Simulation of Compressible Convection. In: Rutten R.J., Severino G. (eds.) Solar and Stellar Granulation. Kluwer, Dordrecht, p. 401
de Boer C.R., 1993, Ph D thesis, Göttingen University
de Boer C.R., 1996, A&AS 120, 195
de Boer C.R., Kneer F., 1992, A&A 264, L24
de Boer C.R., Kneer F., Nesis A., 1992, A&A 257, L4
Denker C., de Boer C.R., Volkmer R., Kneer F., 1995, A&A 296, 567
Druesne P., Borgnino J., Martin F., Ricort G., Aime C., 1989, A&A 217, 229
Elste G., 1968, Solar Phys. 3, 106
Fried D.L., 1966, J. Opt. Soc. Am. 56, 1372
Geltman S., 1962, ApJ 136, 935
Gingerich O., Noyes R.W., Kalkofen W., Cuny Y., 1971, Solar Phys. 18, 347
Harvey J.W., Breckinridge J.B., 1973, ApJ 182, L137
Karpinsky V.N., 1990, Properties of the Solar Granulation. In: Stenflo J.O. (ed.) Proc. IAU Symp. 138, Solar Photosphere: Structure, Convection and Magnetic Fields. Kluwer, Dordrecht, p. 67
Kneer F., Mattig W., Nesis A., Werner W., 1980, Solar Phys. 68, 31
Komm R., Mattig W., Nesis A., 1990, A&A 239, 340
Komm R., Mattig W., Nesis A., 1991a, A&A 243, 251
Komm R., Mattig W., Nesis A., 1991b, A&A 252, 812
Korff D., 1973, J. Opt. Soc. Am. 63, 971
Labeyrie A., 1970, A&A 6, 85
Lohmann A.W., Weigelt G.P., Wirnitzer B., 1983, Applied Optics 22, 4028
Malagoli A., Cattaneo F., Brumell N.H., 1990, ApJ 361, L33
Mehltretter J.P., Mattig W., von Alvensleben A., 1978, Projekt Spektrostratoskop. Eggenstein: ZLDI. Forschungsbericht W78-15
Neckel H., 1996, Solar Phys. 167, 9
Neckel H., Labs D., 1994, Solar Phys. 153, 91
Nesis A., Durrant C.J., Mattig W., 1988, A&A 201, 153
Nesis A., Bogdan T.J., Cattaneo F., et al., 1992, ApJ 399, L99
Nordlund Å., Stein R.F., 1989, Simulating Magnetoconvection. In: Rutten R., Severino G. (eds.) Solar and Stellar Granulation. Kluwer, Dordrecht, p. 453
Pehlemann E., von der Lühe O., 1989, A&A 216, 337
Ricort G., Aime C., 1979, A&A 76, 324
Rodríguez Hidalgo I., Collados M., Vázquez M., 1992, A&A 254, 371
Solanki S.K., Rüedi I., Bianda M., Steffen M., 1996, A&A 308, 623
Spruit H.C., Nordlund Å., Title A.M., 1990, ARA&A 28, 263
Steffen M., Freytag B., Holweger H., 1994, Shocks in the solar photosphere and their spectroscopic signature. In: Schüssler M., Schmidt W. (eds.) Solar Magnetic Fields. Cambridge Univ. Press, p. 298
Vollmöller P., Komm R., Mattig W., 1996, A&A 306, 294
von der Lühe O., 1984, J. Opt. Soc. Am. A1, 510
von der Lühe O., 1993, A&A 268, 374
Weigelt G.P., 1977, Optics Comm. 21, 55
Weigelt G.P., Wirnitzer B., 1983, Optics Letters 8, 389
Wiesmeier A., Durrant C.J., 1981, A&A 104, 207

This article was processed by the author using Springer-Verlag LaTeX A&A style file *L-AA* version 3.